Available online at www.sciencedirect.com

ScienceDirect

St. Petersburg Polytechnical University Journal: Physics and Mathematics 2 (2016) 54–62

www.elsevier.com/locate/spjpm

Many-electron correlations in computations of sodium atom photoabsorption

Alexey V. Konovalov*, Andrey N. Ipatov

Peter the Great St. Petersburg Polytechnic University, 29 Politekhnicheskaya St., St. Petersburg 195251, Russian Federation

Available online 4 March 2016

Abstract

The role of many-electron correlations in photoabsorption processes has been investigated. The results of numerical computations of photoionization cross sections of sodium atom are presented. The many-body effects such as interchannel correlations resulting in autoionization resonance peaks, as well as effects of atomic core polarization were taken into account in the computations in terms of RPAE. Polarization corrections were accounted for using both static and dynamic polarization potentials. The influence of correlations on the position and the form of resonance peaks was studied. The obtained results demonstrate necessity of taking into account polarization effects, especially for clarification of autoionization resonance peaks position and the cross-section magnitudes in the low energy range. The best agreement with experimental data was reached with the model of dynamic polarization potential based on Dyson equation.

Keywords: RPAE; Sodium atom; Dyson equation; Photoabsorption cross section.

Introduction

The rapid advances made in radio astronomy, laser technologies, and optical spectroscopy methods need to be based on sound theoretical foundations for deciphering the experimentally obtained optical spectra of atoms, molecules, atomic clusters, impurities, quantum dots in solid bodies, etc. The correlation effects play a significant role in the interactions between many-body systems; these effects need to be taken into account when constructing a respective theoretical model.

This paper studies the influence of many-electron correlations on the optical properties of atoms using the specific examples of numerical computations of the photoabsorption cross-sections of the sodium atom. The computations were performed taking into account the many-body effects such as interchannel correlations leading to autoionization resonance peaks appearing, as well as the interactions related to atomic core polarization.

The data on the photoabsorption and radiation spectra of atoms offer clues to understanding their structure and the processes occurring when they interact with the electromagnetic field. It should be noted that electron shell structure can be described only through a theory that would adequately interpret the experimental data. The emergence of quantum mechanics,

* Corresponding author.
E-mail addresses: alkonvit@yandex.ru (A.V. Konovalov), andrei_ipatov@mail.ru (A.N. Ipatov).

http://dx.doi.org/10.1016/j.spjpm.2016.02.008

(Peer review under responsibility of St. Petersburg Polytechnic University).

the formulation of the Schrödinger wave equation and its generalizations to many-electron atoms in the form of the Hartree–Fock equations (HF) all once played a key role in understanding the structure of electrons and molecules [1–3]. The HF single-particle approximation allows computing wave functions and energies of the ground and the excited states of many-electron systems. However, this approach has significant disadvantages. The eigenvalues of the Hartree–Fock Hamiltonian mean the ionization energies of the respective electron shells, but, as the computational results indicate, these energies are always substantially different from the corresponding experimental values. Additionally, the excited states are computed in the combined field of the frozen core and the vacancy formed. This means that the wave function of an excited electron is computed without taking into account the rearrangement of the self-consistent field due to a hole appearing in the structure of the electron core and as well as the polarization of the electron core by the knock-on electron. We should note that the methods presented in this study can be applied to describing the optical properties of the individual many-electron atoms as well as of the more complex structures.

The atomic system of units is used in this study: $m_e = |e| = \hbar = 1$.

Theoretical approach

A photoabsorption cross-section of an atom is described by the following formula [2]:

$$\sigma(\omega) = \frac{4\pi^2}{\omega c} \sum_{i \le F} \int \left| \langle v|\hat{M}(\omega)|i\rangle \right|^2 \delta(\omega - E_v + E_i) dv, \tag{1}$$

where F is the highest occupied level (the Fermi level) of the system in its ground state, $\langle v|\hat{M}(\omega)|i\rangle$ is the matrix element of the atomic electron transition from the state i to the state v under the effect of the external electromagnetic field in a dipole approximation.

These single-particle transition amplitudes take into account the change in the state of only one electron, namely, the one interacting with the electromagnetic field. Computations using dipole amplitudes with only the electron–hole interactions taken into account proved this approach to yield an adequate quantitative and qualitative description of the photoabsorption processes only in a limited number of cases. Indeed, the methods based on single-particle approximation cannot provide even a qualitative explanation for some of the observed phenomena, in particular, the autoionization resonance peaks appearing in the partial photoionization cross-sections of outer atomic shells. Because of this, a need arose to further develop the method of the quantum many-body theory.

Random Phase Approximation (RPAE) [2,3,5,6] turned out to be one of the most effective approaches to constructing the operator of the interaction between the atom and the external field; this method allows taking into account many-electron correlations. The photoabsorption cross-sections were first successfully computed in this approximation for a considerable number of atoms with a good agreement between the numerical results and the experimental data. RPAE is based on the assumption that an excited electron is not immediately transferred to the final excited state but instead passes through a number of intermediate short-lived (virtual) ones. The virtual excited states of the electron–hole type interact with the real excitation by the Coulomb field with the exchange interaction allowed for.

The operator form of the expression for the interaction amplitude can be written in RPAE as [5]:

$$\hat{D}(\omega) = \frac{\hat{d}}{1 - \hat{\chi}(\omega)\hat{U}} \tag{2}$$

This expression can also be written in the matrix form as

$$\langle k|\hat{D}(\omega)|i\rangle = \langle k|\hat{d}|i\rangle + \left(\sum_{\substack{k' > F \\ i' \le F}} - \sum_{\substack{i' > F \\ k' \le F}} \right) D_{k'i'} U_{i'kk'i} \chi(\omega)_{k'i'} \tag{3}$$

where

$$D_{k'i'} = \langle k|\hat{D}(\omega)|i\rangle,$$
$$U_{i'kk'i} = \langle i'k|\hat{U}(\omega)|ik'\rangle,$$
$$\chi(\omega)_{k'i'} = \frac{1}{\omega - E_{k'} + E_{i'} + i\delta}.$$

This expression can be also represented by diagrams, as shown in Fig. 1 [5,6]. If the exchange terms are taken out of the sum of Expression (3), the random phase approximation (RPA), widely used in electron gas theory [7], can be obtained.

An important feature of RPAE is the so-called effective interaction appearing in the operator description, different from the pure Coulomb interaction with the core electrons by the adjustments introduced due

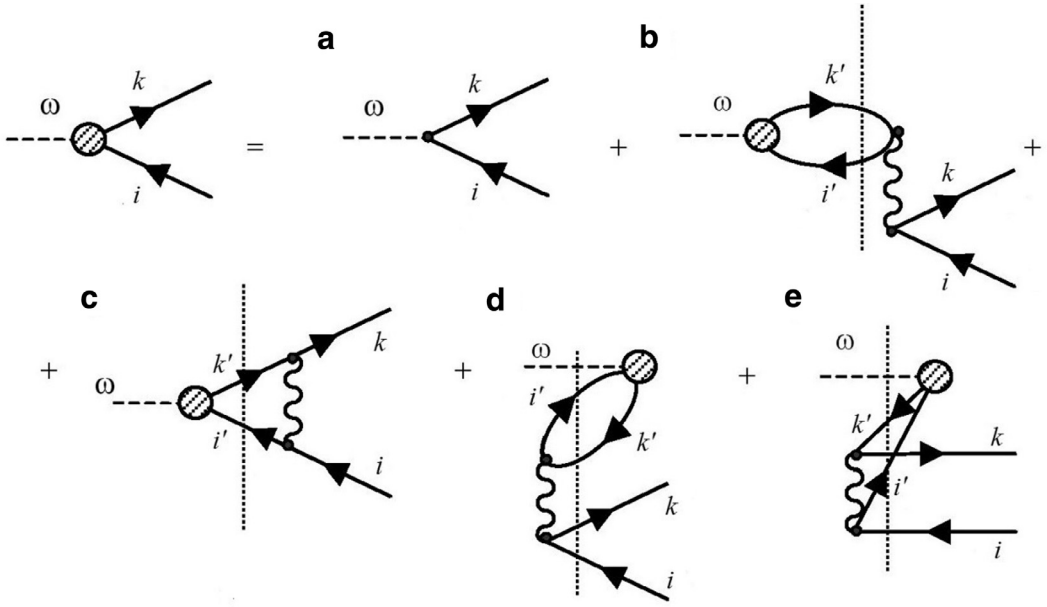

Fig. 1. Diagram representation of the interaction amplitude in RPAE: *a* is the single-particle dipole amplitude; *b* and *c* are the direct and the exchange interactions for the'time-forward' processes; *d* and *e* are the direct and the exchange interactions for the 'time-reverse' processes; ω is the photon frequency; k' and l' are the states of the intermediate (virtual) electron and hole; k and i are the states of the electron and the hole resulting from the photoabsorption process.

to virtual electron–hole excitations emerging [2]:

$$\hat{\Gamma} = \frac{\hat{U}}{1 - \hat{\chi}(\omega)\hat{U}} \tag{4}$$

In matrix form, the expression for the effective interaction elements can be obtained from (3) by substituting the dipole single-particle amplitude with the Coulomb interaction [8,9]:

$$\langle kk'|\hat{\Gamma}(\omega)|ii'\rangle = U_{kk'ii'} + \left(\sum_{\substack{k'' > F \\ i'' \le F}} - \sum_{\substack{i'' > F \\ k'' \le F}} \right) \Gamma_{kk''ii''} U_{i''k'k''k'} \chi(\omega)_{k''i''}, \tag{5}$$

where

$$U_{kk'ii'} = \langle kk'|\hat{U}|ii'\rangle,$$
$$\Gamma_{kk''ii''} = \langle kk''|\hat{\Gamma}(\omega)|ii''\rangle,$$
$$U_{i''k'k''k'} = \langle i''k'|\hat{U}|k''i'\rangle,$$
$$\chi(\omega)_{k'i'} = (\omega - E_{k''} + E_{i''} + i\delta)^{-1}.$$

As mentioned above, RPAE allows describing the profiles of the autoionization resonance lines in the photoabsorption spectra. These phenomena are caused by multi-channel correlations and emerge in the continuous photoionization spectrum of the outer shells in the energy regions close to the energies of discrete transitions from internal shells. The shape of the peak profile can be described by the Fano formula [3,4]:

$$\sigma = \sigma_0 \left(1 - \rho^2 + \rho^2 \frac{(\varepsilon + q)^2}{\varepsilon^2 + 1} \right), \tag{6}$$

where σ_0 is the photoabsorption cross-section in the vicinity of the peak; ρ^2 is the interference index indicating how strongly the channels are involved in the resonance; q is the form index defining the profile of the resonance line.

A dimensionless quantity ε is determined by the ratio

$$\varepsilon = \frac{2(E - E_F)}{\gamma}, \tag{7}$$

where γ is width of the resonance line; E_F is the energy of the discrete transition; the interaction with this transition is taken into account in the process of ionization of the outer shell.

When describing the shape of the autoionization resonance peaks within RPAE, the values γ, E_F, ρ^2, ε, *and* q are expressed through the real and the imaginary parts of the matrix elements of the operators $\hat{D}$ and $\hat{\Gamma}$, and their linear combinations [3].

The correspondence between the computed and the experimental data can also be improved by introducing additional effects caused by the polarization of the

system's electron core. An excited electron creates its own field that distorts the self-consistent field of the atomic core and produces virtual electron–hole pairs interacting with the electron.

One of the methods for taking into account the atomic core polarization and, respectively, its influence on the wave functions of the ground and the excited states is based on using the static effective polarization potential in the following form [3]:

$$V(r) = -\frac{\alpha}{\left(b^2 + r^2\right)^2}, \tag{8}$$

where α is the static dipole polarizability of the atom; b is the phenomenological parameter allowing to avoid divergence at small distances from the atomic nuclei. The dipole polarizability value is typically taken from the experimental data, while the parameter b is selected so that the energy of the outer shell of the ground state could most closely match the experimental ionization energy.

Another approach allowing to take into account the polarization corrections was previously widely used for theoretically studying the scattering of slow electrons by many-electron atoms [8]. The dynamic polarization potential is described by the self-energy part of Green's function for the excited electron, $\Sigma(E,\mathbf{r},\mathbf{r}')$, depending on the energy of the incident electron and two coordinates, i.e., in contrast to the static potential (8), this potential is non-local. The expression for the matrix element $\Sigma(E,\mathbf{r},\mathbf{r}')$ in the second order of the perturbation theory for electron–electron interactions can be written in the form

$$\langle i|\Sigma_E|i'\rangle = \left(\sum_{k_1>F} \sum_{\substack{k_2>F \\ k_3\le F}} + \sum_{k_1\le F} \sum_{\substack{k_2\le F \\ k_3>F}} \right) U_{ik_3k_2k_1} V_{k_1k_2k_3i'} \chi(\omega)_{k_1k_2k_3}, \tag{9}$$

where

$$U_{ik_3k_2k_1} = \langle ik_3|\hat{U}|k_2k_1\rangle,$$
$$V_{k_1k_2k_3i'} = \langle k_1k_2|\hat{V}|k_3i'\rangle,$$
$$\chi(\omega)_{k_1k_2k_3} = \left(\omega - E_{k_1} - E_{k_2} + E_{k_3} + i\delta\left(1 - 2n_{k_1}\right)\right)^{-1}.$$

Here the first parenthetical term corresponds to the 'time-forward' diagrams, and the second one to 'time-reverse' [3,5,6].

The expression (9) is schematically shown in diagrams in Fig. 2. In order to find a new wave function of an electron moving in the field of the polarized core, we used the Dyson equation:

$$\left(\hat{H}^{HF} - E\right)\Psi_E(\mathbf{r}) = \int \Sigma\left(E,\mathbf{r},\mathbf{r}'\right)\Psi_E\left(\mathbf{r}'\right)d\mathbf{r}', \tag{10}$$

where E is the energy of a photoelectron (hole), $\Psi_E(\tilde{\mathbf{r}})$ is its wave function, $\Sigma(E,\mathbf{r},\mathbf{r}')$ is the irreducible self-energy part of Green's function [3,5,6].

Eq. (10) can be rewritten in the form

$$\Psi_E(\mathbf{r}) = \psi_E(\mathbf{r}) + \iint d\mathbf{r}'d\mathbf{r} \int^{\frac{\psi_\gamma(\mathbf{r})\psi_\gamma^*(\mathbf{r}')}{E-\epsilon_\gamma+i0}} \Sigma_E\left(\mathbf{r}',\mathbf{r}''\right)\Psi_E\left(\mathbf{r}''\right)d\epsilon_\gamma, \tag{11}$$

where $\psi_\gamma(\mathbf{r})$ are the single-particle wave functions in the HF approximation corresponding to the $\hat{H}^{HF}$ Hamiltonian and forming a complete set of wave functions; the integration, including all occupied and excited states, is performed over this set.

Using Eqs. (10) and (11), the expression for the matrix element of the dipole operator $\hat{d}$ can be represented in the form

$$\langle\Psi_E|\hat{d}|\Psi_n\rangle = \frac{1}{1+i\pi\langle\psi_E|\tilde{\Sigma}_E|\psi_E\rangle}\left(d_{En} + \int \frac{\tilde{\Sigma}_{E\gamma}d_{\gamma n}}{E-\epsilon_\gamma}d\epsilon_\gamma\right), \tag{12}$$

where

$$d_{En} = \langle\psi_E|\hat{d}|\Psi_n\rangle,$$
$$\tilde{\Sigma}_{E\gamma} = \langle\psi_E|\tilde{\Sigma}_E|\psi_\gamma\rangle,$$
$$d_{\gamma n} = \langle\psi_\gamma|\hat{d}|\Psi_n\rangle.$$

Here $\tilde{\Sigma}_E$ is the reducible self-energy part of Green's function; the integration is once again performed over the whole set of HF states.

This, using Eq. (12), the amplitudes of dipole transitions can be found taking into account the polarization correction based on the dynamic polarization potential model.

It should be noted that this approach can be applied to finding the perturbed states of both the photoelectron and the hole, i.e., it allows to refine the electron core energies of the system's ground state compared to their Hartree–Fock values.

The position of the autoionization resonance peaks in the photoabsorption spectrum depends on the energies of discrete transitions from inner atomic shells. These energies, in turn, typically depend on the spin state of the excited system, For example, in the case of the sodium atom, the line of the autoionization resonance caused by the discrete $2s \rightarrow 3p$ transition is split

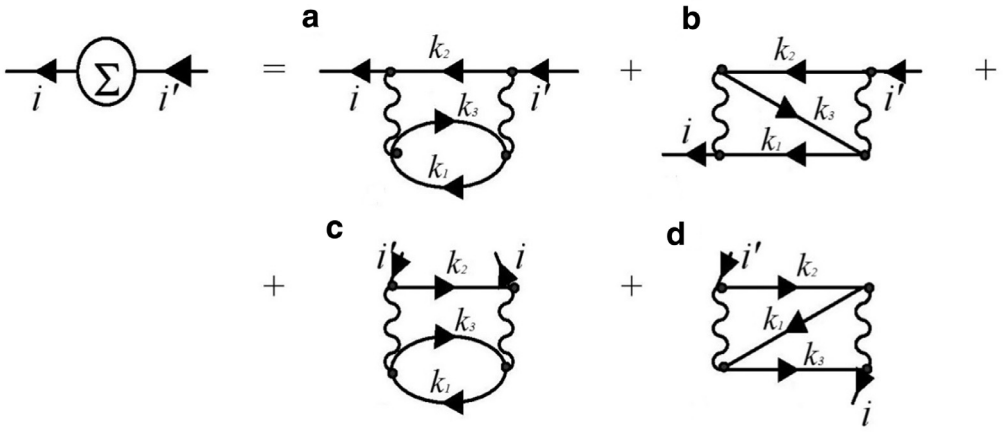

Fig. 2. Diagram representation of a matrix element of the self-energy component of Green's function: *a* and *b* are the direct and the exchange interactions for the 'time-forward' processes; *c* and *d* are the direct and the exchange interactions for the 'time-reverse' processes.

Table 1
Comparison of the computed ionization energies of the sodium atom with the experimental data.

Electron shell	Energy, eV			
	Polarization not taken into account	SPP taken into account	DPP taken into account	Experiment [11]
1*s*	−1101.48	−1101.66	–	−1079
2*s*	−76.11	−76.30	−71.95	−70.90
2*p*	−41.31	−41.50	−38.70	−38.46
3*s*	−4.955	−5.14	−5.14	−5.14

Abbreviations used: SPP is the static polarization potential, DPP is the dynamic polarization potential.

into two peaks whose position corresponds to the final triplet and singlet states. This splitting can be taken into account through the so-called spin-polarized versions of HF and RPAE (SPHF and SPRPAE, respectively), where each atomic shell is divided into two subshells which are filled with electrons with the same spin projections [10].

Discussion of the numerical computation results

The above-described methods were used for computing the photoabsorption cross-sections of the sodium atom. Wave functions and energies of the ground and the excited states were computed within the non-relativistic HF approximation. Table 1 lists the ionization energies of atomic shells computed without and with taking into account the polarization corrections, and the respective experimental values [11].

The experimental value of static dipole polarizability of the ground state of the sodium atom, 162 a.u., was used to construct the effective static polarization potential (8) The parameter $b=11.687$ au was selected in such a way that the computed ionization potential of the $3s$ shell would match the experimental value, equal to −5.14 eV, to a high degree of precision.

The partial and the full photoabsorption cross-sections were computed for photon energies up to 100 eV. Pronounced autoionization peaks were discovered, which proves that taking into account the interchannel correlations is justified when computing the photoionization cross-sections of the outer shells. Four partial ionization channels, $2s \to np$, $2p \to ns$, $2p \to nd$ and $3s \to np$, were taken into account when numerically modeling the photoexcitation process for the sodium atom (the $1s \to np$ channel was not taken into account, since the ionization energy of the 1 s shell falls outside the energy range under consideration).

Transition amplitudes and partial cross-sections were computed within RPAE for photon energies up to 100 eV. In order to refine the numerical results, amplitudes and cross-sections were also computed using wave functions obtained taking into account the polarization corrections. The shape and the precise location of the autoionization peaks caused by the discrete $2s \to 3p(^2P)$, $2s \to 3p(^1P)$, $2s \to 4p(^2P)$

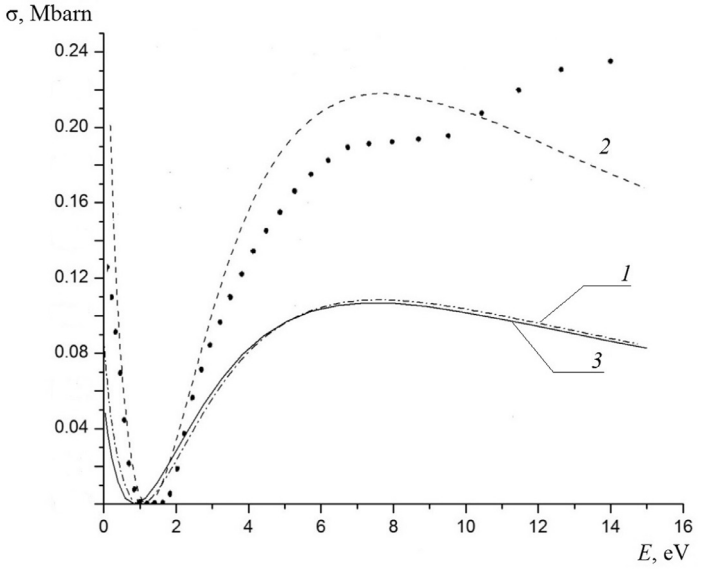

Fig. 3. The computed (lines) and the experimental (dots) curves of the full photoabsorption cross-section of the sodium atom versus the photoelectron energy. Various approximations were used: RPAE taking into account the static polarization potential (*1*), SPRPAE taking into account the dynamic polarization potential (*2*), RPAE without polarization (*3*).

and $2s \to 4p(^1P)$ transitions were computed within the SPRPAE approach.

The accuracy with which the computed and the experimental positions of the Cooper minima coincide is one of the criteria indicating that the computation is valid [3]. Fig. 3 shows the photoabsorption cross-sections of the sodium atom versus the photoelectron energies. It is evident from the dependences presented that taking into account the polarization corrections allows to improve the fit between the computed and the experimental [12,13] positions of the Cooper minima. However, a significant improvement of the fit between the experimental and the computed photoabsorption cross-sections was obtained only when the dynamic polarization potential model was used.

Fig. 4 shows the total cross-sections versus the photoelectron energies. As seen from the experimental dependence published in Ref. [14], the photoionization intensity is relatively small for photon energies lower than 38.5 eV, since only the electron from the outer 3*s*-shell participates in the ionization process in this energy range. Energy regions where the autoionization resonance peaks are located are the exception. For example, a particularly intense peak caused by the resonance interaction with the discrete $2p \to 3s$ excitation is observed at an energy of 31 eV.

The shape and the location of this peak were examined, and the parameters necessary for constructing the Fano profile (6) were computed (see Table 2).

The computed peak location is in good agreement with the experiment; unfortunately, however, since it is narrow and highly intense, no specific conclusions can be drawn regarding the coincidence of the height and the shape. The computed resonance lines and their respective Fano profiles are shown in Fig. 5

Very narrow and closely spaced peaks caused by the resonance of the $3s \to np$ channel with discrete $2p \to ns$ and $2p \to nd$ transitions are observed in the 33.0–38.5 eV region. Above the energy of 38.5 eV corresponding to the bonding energy of the 2*p*-shell, the ionization of this shell starts occurring in two channels, $2p \to ns$ and $2p \to nd$. A number of peaks are observed in the 38.5–45.5 eV energy range in the experimental cross-section, which can be attributed to two-electron excitations characterized by the simultaneous excitation of the 2*p* and the 3*s*-shell electrons [14].

Furthermore, above 70.9 eV, the photoionization of the 2*s*-shell starts. The excitations of the 2*s*-electrons in the continuous spectrum contribute insignificantly to the total photoionization cross-section; however, the discrete $2s \to 3p$ and $2s \to 4p$ transitions cause autoionization resonance peaks to emerge in the 63–71 energy range.

Numerical computations were performed; the shapes and the locations of the autoionization resonance peaks caused by the interactions with the discrete $2s \to 3p$ and $2s \to 4p$ transitions were examined.

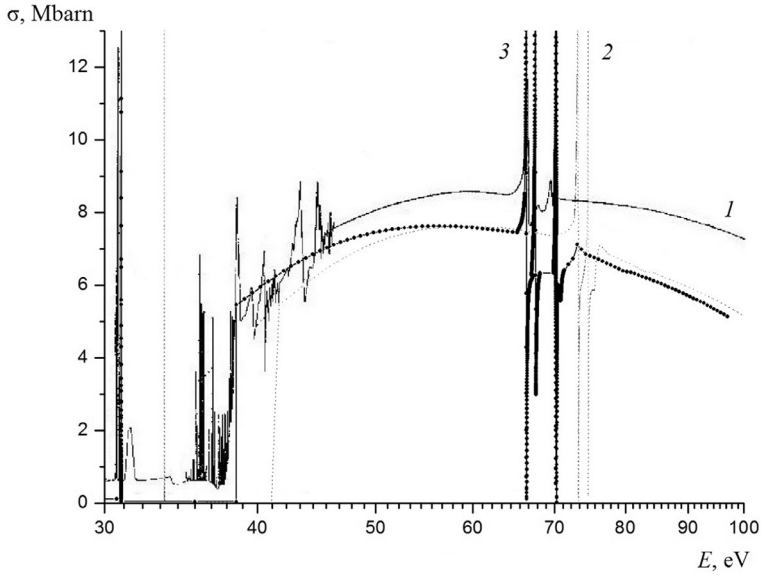

Fig. 4. The experimental [14] (*1*) and the computed curves of the full photoabsorption cross-section of the sodium atom versus the photon energy. Various approximations were used: RPAE without polarization (*2*) and SPRPAE taking into account the dynamic polarization potential (*3*).

Table 2
The computed parameters for constructing the Fano profiles.

Electron transition	Transition energy E_F, eV	Line width γ, 10^{-3}eV	Asymmetry parameter q
$2p \to 3s$	30. 96	0.14	−754.34
$2s \to 3p(^2P)$	66.37	34.4	−1.60
$2s \to 3p(^1P)$	67.59	39.6	−1.64
$2s \to 4p(^2P)$	70.29	8.2	−1.80
$2s \to 4p(^1P)$	70.18	6.1	−1.70

It can be seen from the experimental curve [14] that each of these peaks is in turn split into two lines corresponding to a specific spin state, i.e. the triplet and the singlet. Because of this, the locations of these peaks were computed within SP RPAE. The computations performed in this approximation showed that the discrete $2s \to 3p(^2P)$, $2s \to 3p(^1P)$, $2s \to 4p(^2P)$ and $2s \to 4p(^1P)$ transition energies were equal to 70.53, 71.75, 74.45 and 74.34 eV, respectively. Consequently taking into account the dynamic polarization potential allowed shifting the location of the 2*s*-level from the energy of –76.11 eV to–71,95 eV, i.e., the transition energies decreased by 4.16 eV and became equal to 66.37, 67.59, 70.29 and 70.175 эВ,eV, respectively.

Remarkably, according to the computations performed, the singlet-state energy for the $2s \to 4p$ transition proved to be lower than the triplet-state one. This fact needs to be rechecked using the multiconfiguration Hartree–Fock approximation. There are discrepancies in the experimental and the computed peak shapes. The computed ones turned out to be more intense, and there is a characteristic dip in the photoabsorption cross-sections after each peak. This is possibly because an insufficiently small energy step was taken when the experiment was carried out in this energy range. In particular, this would explain the absence of the autoionization resonance peaks caused by the discrete $2s \to 5p$, $2s \to 6p$, etc., transitions on the experimental curve.

It should be noted that taking into account the polarization corrections does not lead to a significant improvement in the agreement between the experimental and the computed cross-sections in the 30–100 eV energy range; it does, however, allow to refine the locations of the autoionization resonance peaks and the ionization thresholds of shells. Introducing the polarization corrections using the dynamic polarization potential in the 5.14–20.14 eV range turned out to be justified as it improved the agreement between the computed and the experimental

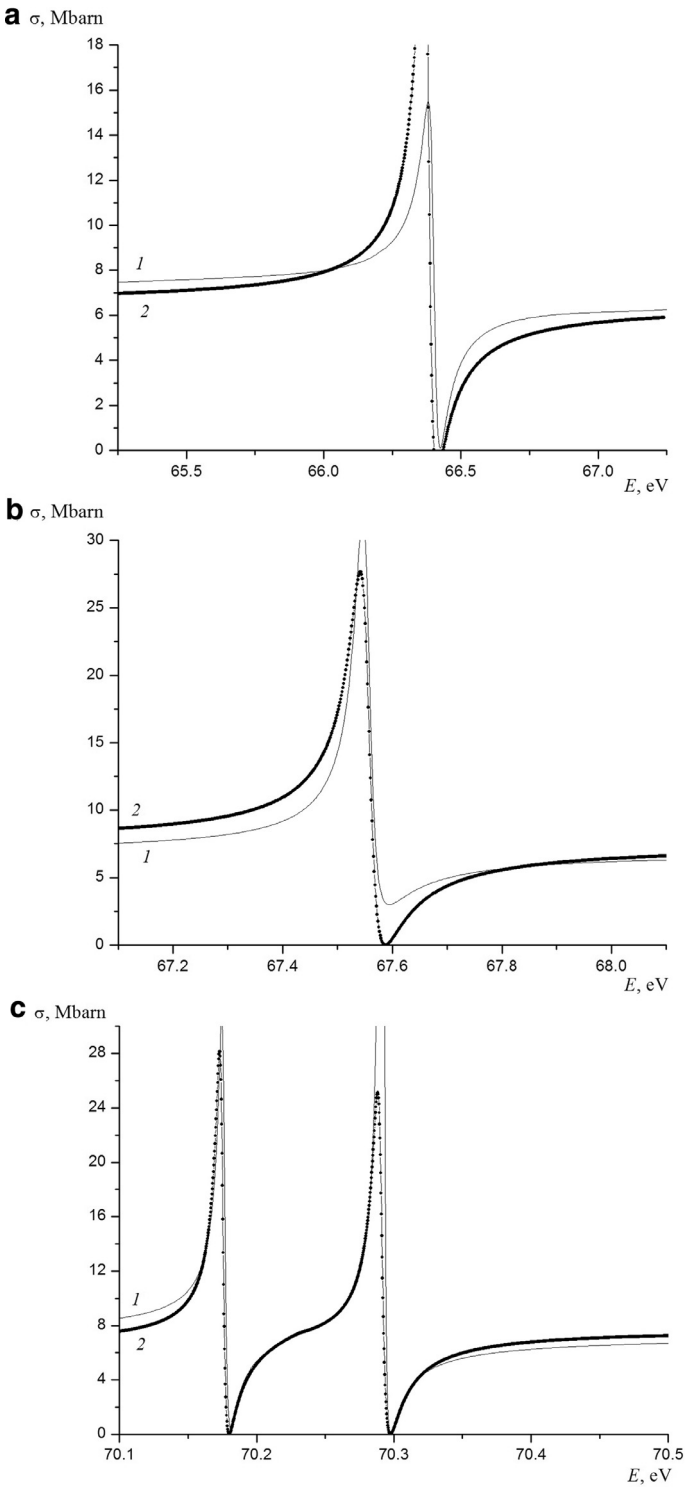

Fig. 5. The computed autoionization resonance spectrum (*1*) and the corresponding Fano profiles (*2*). Resonance peaks corresponding to $2s \to 3p(^2P)$ (*a*), $2s \to 3p(^1P)$ (*b*), $2s \to 4p(^1P)$ and $2s \to 4p(^2P)$ (*c*) are shown.

results. Therefore, we can conclude that the effects related to atomic core polarization have a significant effect on the transition amplitudes only at low photoelectron energies. Unfortunately, the obtained computed photoabsorption cross-section is different from the experimental one, and this discrepancy grows with an increase of the photon energy. The agreement between the cross-sections is 80–90% in the 45–64 eV energy range, and decreases to 70% in the 70–100 eV range. Presumably, this could be due to the fact that the computations were performed in a non-relativistic approximation. It is possible that using the Hartree–Fock–Dirac approximation for computing electron wave functions could improve the agreement between the computations and the experiment.

Conclusion

The Hartree–Fock approach was used for finding wave functions and single-electron energies of the sodium atom in the ground and the excited states. The photoionization amplitudes and the photoabsorption cross-sections for this atom were computed through RPAE which explains the experimentally observed autoionization resonance peaks emerging. The polarization corrections necessary for refining the energies and the wave functions of the ground and the excited states were taken into account by various methods, in particular, by the effective static polarization potential model and by the model using the dynamic polarization potential. Comparing the computed and the experimental data proves that it is necessary to take into account the electron–electron correlations in order to qualitatively describe the optical properties of the atoms; it is also useful to take into account the polarization corrections when refining the photoabsorption cross-sections and the ground state energies. In particular, introducing the dynamic polarization potential allowed to significantly improve the agreement between the locations of the autoionization resonance peaks and the experimental data; however, using this method to refine the photoabsorption cross-sections only proved justified for the case of low energies. Possibly, using a relativistic basis may improve the agreement between the computed and the experimental data in the high-energy range. In order to further refine the positions of the autoionization resonance peaks, it is necessary to go beyond the Hartree–Fock approach, in particular, by using the multi-configuration Hartree–Fock approximation and its relativistic generalization. The RPAE method can be applied not only to describing atoms, but also molecules, clusters, and other nanostructures [14–17].

The authors express their gratitude to Professor V.K. Ivanov, Doctor of Physical and Mathematical Sciences, for his help in preparing the paper and the fruitful discussion of the obtained results.

References

[1] D. Hartree, The Computation of Atomic Structures, Chapman A;. HALL, LTD, London, 1957.
[2] M.Ya. Amusia, L.V. Chernysheva, Computation of Atomic Processes (1997).
[3] M.Ya. Amusya, Atomic Photoeffect, Plenum Press, New-York, 1990.
[4] U. Fano, L. Fano, Physics of Atoms and Molecules: An Introduction to the Structure of MattER, Chicago University Press, Chicago, 1972.
[5] M.Ya. Amusya, V.K. Ivanov, N.A. Cherepkov, L.V. Chernysheva, Processes in Multielectron Atoms, Nauka, St. Petersburg, 2006.
[6] V.K. Ivanov, A.N. Ipatov, R.G. Polozkov, Many-Body Quantum Theory, Polytechnical University Publishing House, St. Petersburg, 2013.
[7] S. Lundquist, N.H. March, Theory of the Inhomogeneous Electron Gas, Plenum Press, New York-London, 1983.
[8] M.Ya. Amus'ya, N.A. Cherepkov, L.V. Chernysheva, Cross section for the photoionization of noble-gas atoms with allowance for multielectron correlations, J. Exp. Theoret. Phys 33 (1) (1971) 90–96.
[9] M.Ya. Amusya, V.K. Ivanov, Intershell interaction in atoms, Physics-Uspekhi (Adv. Phys. Sci.) 152 (6) (1987) 185–230.
[10] M.Ya. Amusya, V.K. Dolmatov, V.K. Ivanov, Photoionization of atoms with half-filled shells, J. Exp. Theoret. Phys. 85 (1) (1983) 115–123.
[11] A.A. Radtsig, B.M. Smirnov, Parameters of Atoms and Atomic Ions, Energoatomizdat, Moscow, 1986.
[12] A. Dasgupta, A.K. Bhatia, Photoionization of sodium atoms and electron scattering from ionized sodium, Phys. Rev. A. 31 (2) (1985) 759–771.
[13] Jwei-Jun Chang, Hugh P. Kelly, Photoabsorption of the neutral sodium atom: a many-body computation, Phys. Rev. A. 12 (1) (1974) 92–98.
[14] H.F. Wolff, K. Radler, B. Sonntag, R. Haensel, Photoabsorption of atomic sodium in the VUV, Z. PhysikA. 257 (4) (1972) 353–368.
[15] S.K. Semenov, N.A. Cherepkov, Generalization of the atomic RPA method for diatomic molecules: H_2 photoionization cross-section computation, Chem. Phys. Lett. 291 (3-4) (1998) 375–380.
[16] S.K. Semenov, N.A. Cherepkov, Photoionization of the H_2 molecule in the random phase approximation, J. Phys. B. 36 (7) (2003) 1409–1422.
[17] S.K. Semenov, N.A. Cherepkov, G.H. Fecher, G. Schönhense, Generalization of the atomic random-phase-approximation method for diatomic molecules: N_2 photoionization cross–section computations, Phys. Rev. A. 61 (3) (2000) 032704.